SANDIA REPORT
SAND2007-0036
Unlimited Release
Printed January 2007

The Strain-Rate Sensitivity of High-Strength High-Toughness Steels

Brad L. Boyce, Thomas B. Crenshaw, and Morris F. Dilmore

Prepared by
Sandia National Laboratories
Albuquerque, New Mexico 87185 and Livermore, California 94550

Sandia is a multiprogram laboratory operated by Sandia Corporation,
a Lockheed Martin Company, for the United States Department of Energy's
National Nuclear Security Administration under Contract DE-AC04-94AL85000.

Issued by Sandia National Laboratories, operated for the United States Department of Energy by Sandia Corporation.

Available to DOE and DOE contractors from
U.S. Department of Energy
Office of Scientific and Technical Information
P.O. Box 62
Oak Ridge, TN 37831

Telephone: (865) 576-8401
Facsimile: (865) 576-5728
E-Mail: reports@adonis.osti.gov
Online ordering: http://www.osti.gov/bridge

Available to the public from
U.S. Department of Commerce
National Technical Information Service
5285 Port Royal Rd.
Springfield, VA 22161

Telephone: (800) 553-6847
Facsimile: (703) 605-6900
E-Mail: orders@ntis.fedworld.gov
Online order: http://www.ntis.gov/help/ordermethods.asp?loc=7-4-0#online

SAND2007-0036
Unlimited Release
Printed January 2007

The Strain-Rate Sensitivity of High-Strength High-Toughness Steels

B. L. Boyce and T. B. Crenshaw
Materials Science and Engineering
Sandia National Laboratories
P.O. Box 5800
Albuquerque, NM 87185-0889

M. F. Dilmore
AFRL/MNMW
Eglin AFB, FL

Abstract

The present study examines the strain-rate sensitivity of four high strength, high-toughness alloys at strain rates ranging from 0.0002 s^{-1} to 200 s^{-1}: Aermet 100, a modified 4340, modified HP9-4-20, and a recently developed Eglin AFB steel alloy, ES-1c. A refined dynamic servohydraulic method was used to perform tensile tests over this entire range. Each of these alloys exhibit only modest strain-rate sensitivity. Specifically, the strain-rate sensitivity exponent *m*, is found to be in the range of 0.004 – 0.007 depending on the alloy. This corresponds to a ~10% increase in the yield strength over the 7-orders of magnitude change in strain-rate. Interestingly, while three of the alloys showed a concominant ~3-10% drop in their ductility with increasing strain-rate, the ES1-c alloy actually exhibited a 25% increase in ductility with increasing strain-rate. Fractography suggests the possibility that at higher strain-rates ES-1c evolves towards a more ductile dimple fracture mode associated with microvoid coalescence.

Acknowledgements

The authors would like to thank V. Luk, D. Dederman, and D. Frew for their administrative and fiscal support for this project under the auspices of the DOD/DOE MOU TCG XI. BLB would like to thank R. Grant for SEM documentation of fracture surfaces, and would also like to thank Prof. D. Matlock of the Colorado School of Mines for fruitful discussions on this topic.

Contents:

1. Introduction

Reliable design of structural components requires an understanding of their material properties *under relevant conditions*. In the case of earth-penetrating munitions or gravity-dropped weapons, which are traditionally constructed from high-strength, high-toughness steels, this requires an understanding of the dynamic mechanical properties at relevant strain-rates. Specifically, these types of impact environments typically involve impact durations where the maximum strain is reached within ~1 ms of initial contact. In a metal which undergoes 50% strain, such an impact corresponds to a strain rate of 500 s^{-1}. The focus of the present study is to establish the rate-dependent tensile behavior of several high-strength steel alloys at strain rates approaching this regime.

There is very limited data available in the literature regarding deformation behavior at strain rates in the range of 10-500 s^{-1}. This is partially due to the difficulty in testing in this "intermediate" or "sub-Hopkinson" strain-rate regime, where rates are faster than the traditional quasi-static equilibrium of a conventional stress- or strain-controlled tensile test and slower than the single-wave mechanics of a split-Hopkinson bar test. These difficulties have led to numerous published datasets of questionable validity, where undesired "oscillations" or "ringing" in the force signal were merely smoothed numerically after the test. The present study employs recently developed damping and robust load cell design to greatly mitigate these convoluting effects.

One of the most notable datasets in the literature regarding the behavior of steels in the sub-Hopkinson rate regime was published by Bleck and Schael in 2000 [1]. The authors were themselves aware of the challenge of accurately testing at these intermediate rates, noting: "*At high strain rates the force signal was superimposed by oscillations caused by the inertia of the test equipment making the direct determination of characteristic values impossible. Therefore a cubic spline was utilized to approximate the unfiltered stress-strain signal...*". In spite of these limitations, their compiled results provide a snapshot as to the possible expectations for changes in mechanical behavior at intermediate rates. As shown in Figure 1, their study examined the strain-rate sensitivity of a wide range of steels including austenitic stainless steels (1.4301, 1.4318), TRIP steel, dual-phase steels (DP600, DP800, DP1000), a high-strength steel (ZStE340), and a deep-drawing grade (DC04). All of the alloys showed a similar expected strain-rate dependence on yield strength: shallow at low rates, and ever steeper with increasing strain rate. The strongest alloy, DP1000 with a yield

strength of ~620 MPa at 0.005 s^{-1}, showed the most dramatic strain-rate sensitivity on yield strength, increasing to 900 MPa at the dynamic rate ~200 s^{-1}. Ductility behavior was less consistent: the austenitic stainless alloys showed marked loss of ductility as strain rate rose from 0.005 s^{-1} to 1 s^{-1}, whereas other alloys either showed essentially no ductility change, or only showed significant changes in ductility at the faster strain rates. The previous study on behavior of steels in the sub-Hopkinson regime suggests that these alloys become most strain-rate sensitive only at the highest strain-rates approaching ~200 s^{-1}. Thus, had their study only extended to 10 s^{-1}, a typical limit for many previous conventional strain-rate sensitivity studies, much of the dynamic strengthening effect would not have been observed. This result provides additional motiviation for characterizing the mechanical response of impact-susceptible structural materials at the strain-rates of relevance.

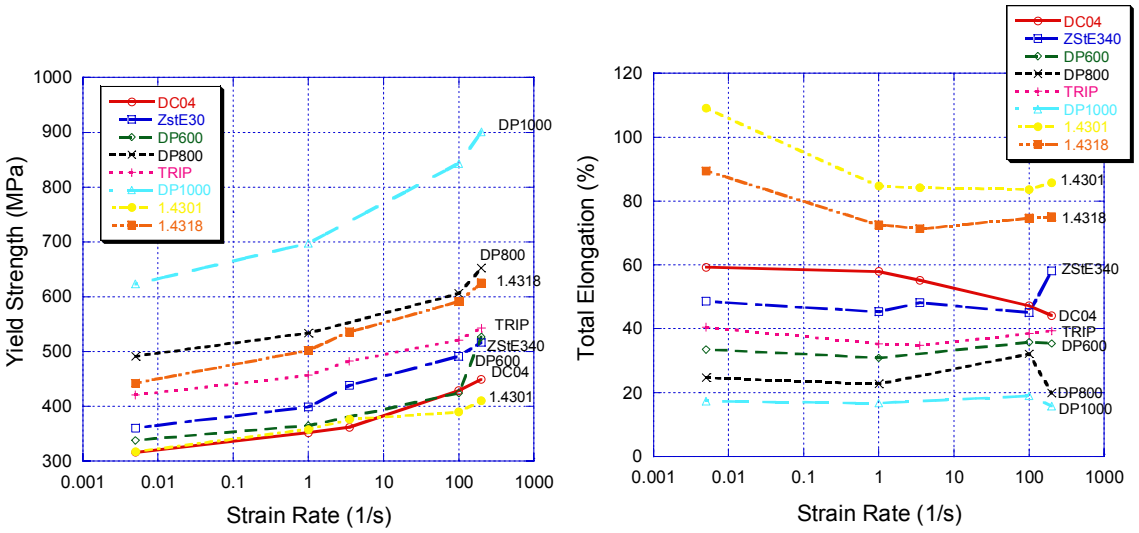

Figure 1. *Strain-rate sensitivity in the sub-Hopkinson regime for several European ferrous alloys. Based on Ref. [1].*

2. Materials

Four high-strength steel alloys were considered in this evaluation: one commercial alloy, Aermet 100; two modified alloys based on commercially available products: 4340M (modified based on AISI 4340) and 9420M (modified based on HP9-4-20); and one newly developed graded, ES-1c. The compositions of the alloys are listed in Table 1. Aermet 100 was supplied by Carpeneter Steel and the other three alloys were obtained as development heats by AFRL. Each of these four alloys are under consideration for emerging earth penetrating munitions applications.

Table 1. *Composition of four high-strength steel alloys*

	ES1-c	4340M	HP9-4-20M	Aermet 100
C	0.26	0.33	0.18	0.22
Mn	0.65	0.75	0.3	0.01
Si	1	0.25		0.03
Ni	1	2.3	9	11.22
Cr	2.6	1.1	0.75	3.01
Mo	0.42	0.45	1	1.16
Co			4.5	13.46
W	1.0			
V	0.07	0.1	0.12	

The heat treatments used for the alloys are as follows:

ES1-C (1) Ramp temperature to 1200F@220F/hour and hold for 5 hours, ramp to austentizing temperature of 1750F@220F/hour; hold for 20 minutes for the first inch of thickness and increase the hold temperature by 10 minutes/inch for each additional inch of thickness (minimum hold temperature of 30 minutes.). (2) Oil quench to 200F and place in 400F furnace. Increase tempering temperature to 500F@100F/hour and hold for 4 hours, air cool.

4340M (1) Ramp to normalizing temperature of 1650F@220F/hour; hold for 1 hour for the first inch of thickness and increase the hold temperature by 1 hour/inch for each additional inch of thickness (minimum hold temperature of 1 hour) and air cool. Ramp to the austentizing temperature of 1525F@220F/hour; hold for 1 hour for the first inch of thickness and increase the hold temperature by 1 hour/inch for each additional inch of thickness (minimum hold temperature of 1 hour). (2) Oil quench to 200F and place in 500F furnace; increase tempering temperature to 925F@100F/hour and hold for 3 hours, air cool.

HP9-4-20M (1) Ramp to normalizing temperature of 1650F@220F/hour; hold for 1 hour for the first inch of thickness and increase the hold temperature by 1 hour/inch for each additional inch of thickness (minimum hold temperature of 1 hour) and air cool. Ramp to the austentizing temperature of 1550F@220F/hour; hold for 1 hour for the first inch of thickness and increase the hold temperature by 1 hour/inch for each additional inch of thickness (minimum hold temperature of 1 hour). (2) Oil quench to 200F and place in 500F furnace; increase tempering temperature to 1050F@100F/hour and hold for 3 hours, air cool.

Aermet 100 Ingot supplied are vacuum induction melted/vacuum arc re-melted (VIM/VAR). Ramp furnace to the austentizing temperature of 1625F and hold for 1 hour, air cool, refrigerate at -100F for 1 hour, air warm, temper at 900F for 5hours and air cool.

Aermet 100 (UNS K92580) is presently the "gold standard" for steels possessing a combination of exceptionally high strength and toughness. Aermet 100 is a one of the newest alloys in a lineage of secondary hardening Ni-Cr-Mo-Co steels, originally developed in the early 1970's, including HP9-4-20, HY180, AF1410, and Aermet 310. The alloying elements in these Ni-Cr-Mo-Co steels impart the high strength and high toughness while maintaining admirable stress-corrosion cracking properties (K_{Iscc} ~35 ksi√in for Aermet 100), good hardenability for large section sizes, and good weldability. These alloys typically contain 9-11% Ni, which improves toughness, improves strength by solid solution, promotes hardenability, and lowers the ductile-to-brittle transition temperature to well below room temperature. Cr and Mo promote hardenability and strength without contributing to embrittlement. Co additions result in a much more pronounced secondary-hardening peak, thereby contributing substantially to strength for tempering temperatures in excess of 400°F. Further details of the metallurgy associated with these steels can be found in Ref. [2].

The primary limiting factor in the selection of Aermet 100 for many structural applications is the cost. In 2002, the ingot price for Aermet 100 was ~$10/lb. This cost is largely driven by the cost of expensive alloying elements, i.e. cobalt and nickel, and also by the proprietary protection of the alloy. HP9-4-20, an alternative alloy from the same genre as Aermet 100 with less nickel and cobalt, costs less than half that of Aermet 100, and therefore receives consideration in spite of its somewhat diminished strength values. More traditional quench and temper steels, such as 4340 (UNS J24055) can provide reasonable combinations of strength and toughness at a much reduced cost due to the lack of expensive alloying elements, and the relatively simple processing requirements.

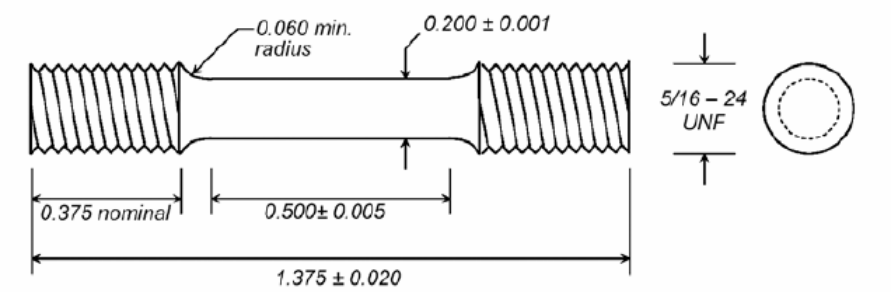

Figure 2. *Cylindrical threaded tensile bar design. Dimensions are in inches.*

3. Testing Method

Cylindrical threaded dogbone tensile bars were extracted from the longitudinal axis of parent billet material, as shown in Fig. 2. The gage section of the tensile bars was only 0.5 inches long so that a strain rate of ~200 s^{-1} could be obtained for a displacement rate of 100 inch/s.

All tensile tests were performed on a MTS servohydraulic loadframe controlled by an MTS 458 analog controller; the loadframe includes integrated high-speed actuator and hydraulic pressure accumulators capable of displacement rates from quasi-static to over 300 inch/s. This servohydraulic tensile method permitted both the load frame configuration and the specimen design to remain constant at all strain rates ranging from <0.00001 s^{-1} to >200 s^{-1}, thereby eliminating potential errors induced by changes in the test set-up. High-speed tests required a so-called "slack adapter", shown in Fig. 3, which permitted >2 inches of actuator travel before load was applied to the tensile bar, so that the actuator could attain its desired velocity prior to the start of the tensile test.

The most challenging aspect of dynamic tensile testing at strain rates in the range of 10-1000 s^{-1} is the control and mitigation of dynamic elastic stress waves which propagate through the specimen, loadcell, and test frame. These stress waves can produce (a) inhomogeneous stresses within the tensile bar, (b) time-dependent oscillations in stresses within the tensile bar, and/or (c) apparent time-dependent oscillations in force as measured by the load cell. To mitigate these effects, a 0.25-inch thick piece of rubber was used at the interface between the slack-adapter pin and the lower specimen grip which minimized the generation of high-amplitude elastic stress waves generated by initial impact. Also, two resonance-resistant custom made load cells were employed directly at either end of the tensile bar to ensure dynamic equilibrium. These load cells proved to dramatically reduce apparent force oscillations compared to off-the-shelf dynamic quartz load washers, as shown in Fig. 4. Further details of the test setup and design can be found in Ref. [3].

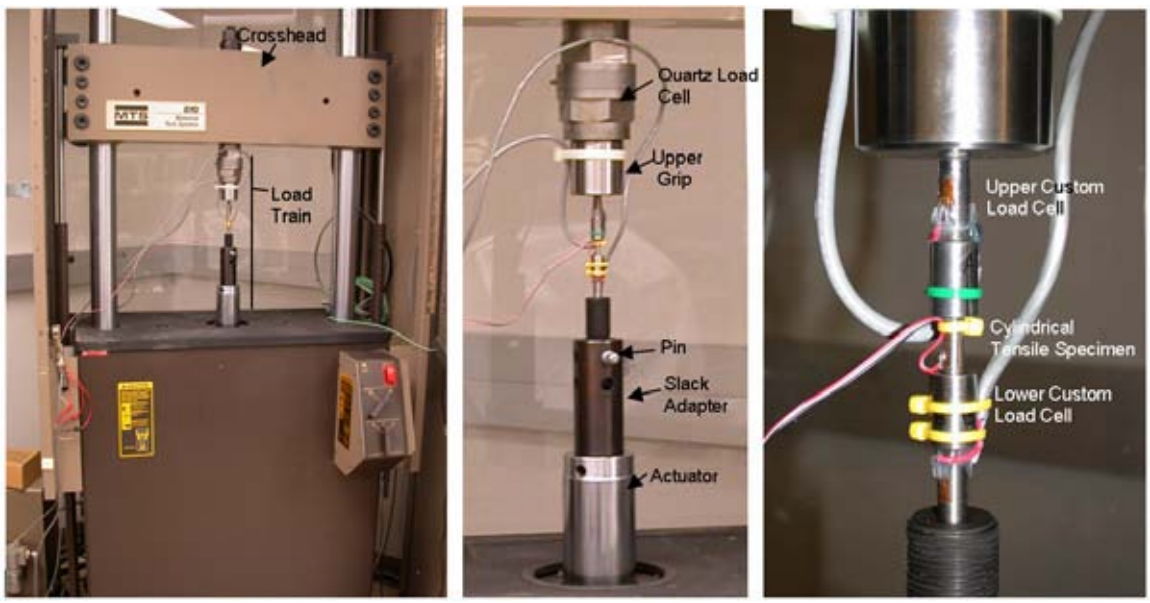

Figure 3. *Experimental configuration with two custom load cells and a standard quartz load cell.*

Strain was measured with a Vishay Micromeasurments Group high-elongation uniaxial strain gage affixed to the middle of the gage section. The load cell and strain gage signals were conditioned and amplified by a Vishay Micromeasurements Group 2300-series amplifier. Data was collected by a triggered Tektronix TDS-3014B digital storage oscilloscope for dynamic tests, or by a Data Translations 12-bit USB data acquisition card for the slow tests which lasted >60s.

Data analysis is summarized in Fig. 4 using the example of a HyTuf alloy at a nominal actuator displacement rate of 280"/sec. Fig. 4a shows the force-time profile from both upper and lower custom-made load cells, showing reasonably good agreement and minimal oscillations compared to the off-the-shelf quartz cell. This plot also shows the linear displacement-time profile for the actuator travel. The entire duration of the test from elastic loading to fracture was less than 0.5 ms. In Figs. 4b-d, a similar test is shown with data from a high-elongation strain gage attached to the gage-section of the test sample. In Fig. 4b, the strain signal is non-linear during initial load up, as the rubber pad is compressed. This ramp in strain-rate during elastic loading dampens inertial shock in the system. From this direct measure of strain, we can determine that the strain-rate at yield in the gage section was ~500 s^{-1}, which is consistent with the displacement rate of 280"/sec and the gage length of 0.5". Figs 4c and 4d show the engineering stress-strain behavior and the extraction of the 0.2% offset yield strength, respectively.

Post-mortem fractographic analysis was performed with a JEOL JSM-5900LV scanning electron microscope (SEM) with a tungsten filament. Also, reduction in area and total elongation of the tensile bars were determined using optical metrology on fiduciaries within the gage section.

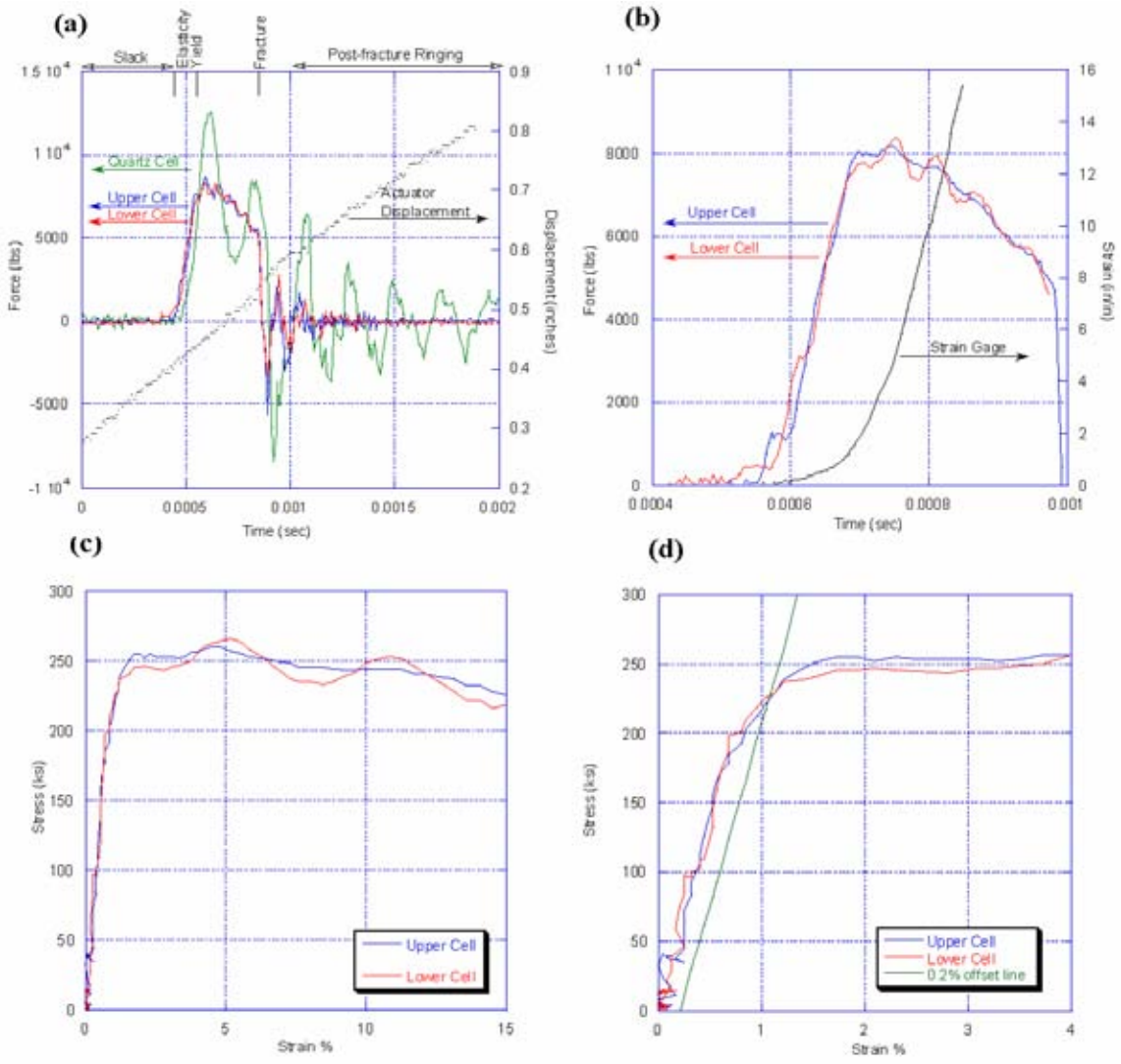

Figure 4. ***(a)*** *Force-time profile from a tensile test on a Hy-Tuf alloy at a displacement rate of ~280"/sec showing the improved quality of the custom load cells over the quartz load cells and showing the linearity of the displacement ramp over the test duration.* ***(b)*** *Force-time profile from a similar test at 280"/sec on Hytuf showing the strain signal from the gage section,* ***(c)*** *data from (b) plotted as stress-strain,* ***(d)*** *0.2% offset line used to determine yield stress.*

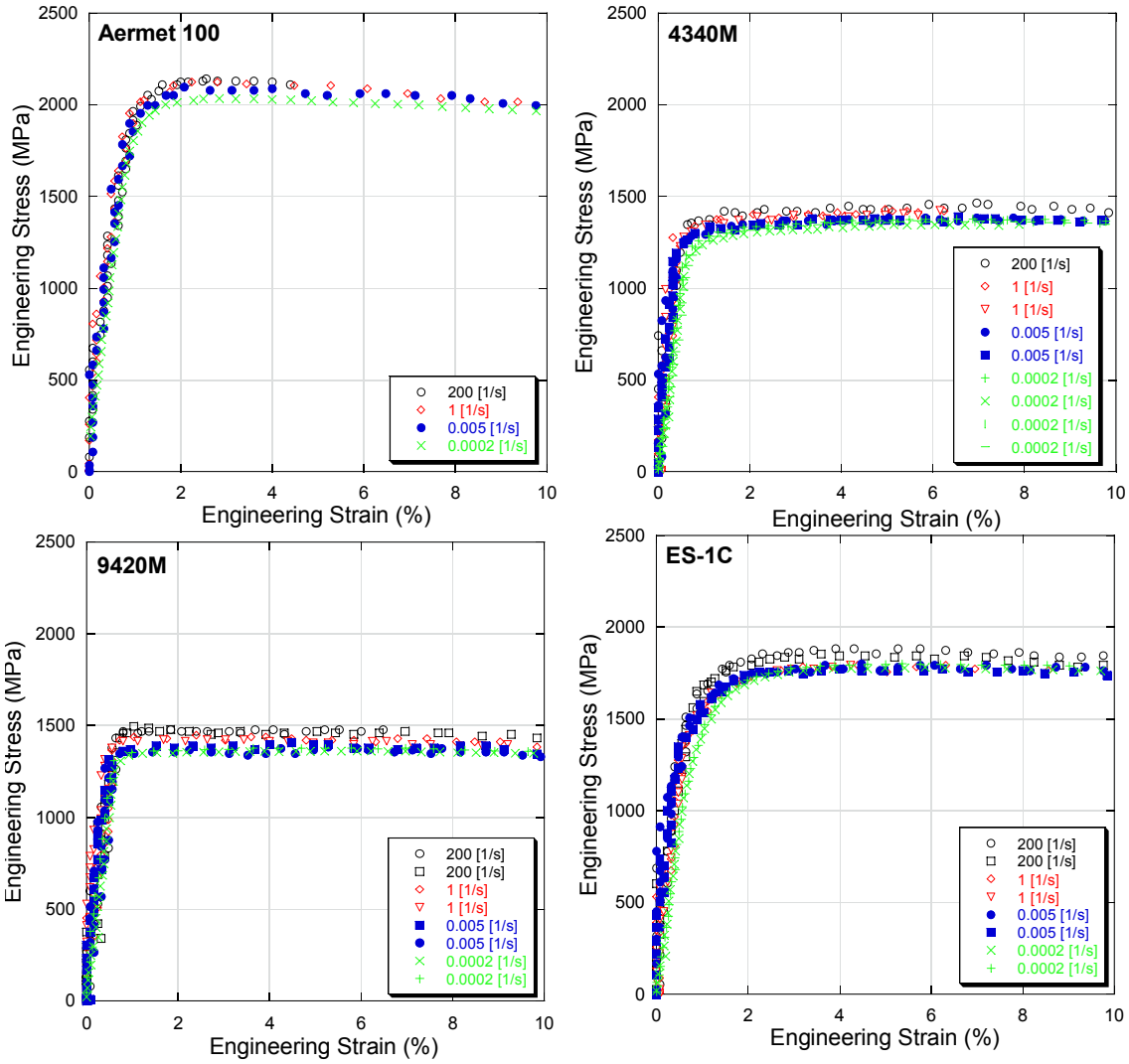

Figure 5. *Engineering stress-strain curves for the four high-strength steel alloys under evaluation at strain rates ranging from 0.0002* s^{-1} *to 200* s^{-1}.

4. Results

The engineering stress-strain curves obtained on each of the four alloys are shown in Figure 5 for strain rates ranging from quasi-static (0.0002 s^{-1}) to dynamic (200 s^{-1}). The data shown in Figure 5 only extend to strains of 10%: the high-elongation strain gages were unreliable at higher strains, which prevented the determination of the entire stress-strain curve. For the three of the alloys supplied by AFRL (4340M, HP9-4-20M, and ES-1c), at least two tests were completed for each test condition, thereby providing evidence of reproducibility. It is clear from this Figure that all four alloys showed a slight increase in

yield strength with strain rate over the 6 orders of magnitude that were spanned in this study. The strength increase, while small, could be clearly distinguished from specimen-to-specimen scatter. Work-hardening rate appeared to be largely unaffected by strain-rate. Also, other characteristic features were seen at all strain-rates: for example, ES1-c showed noticeable curvature in the stress-strain curve at yield whereas 9420M showed a sharp transition from elasticity to plasticity.

A more succinct picture of the strain-rate sensitivity of these alloys can be obtained by examining the trends in yield and ultimate strength as a function of strain-rate, shown in Figure 6. For each of these trends, a somewhat arbitrary trendline is included to help distinguish the datasets. From this plot, each of the four alloys show a ~150 MPa increase in yield strength from 0.0002 s^{-1} to 200 s^{-1}, and a somewhat smaller increase in ultimate strength over the same range. 4340M, HP9-4-20M, and ES-1c all showed the expected non-linear strain-rate trend which was shallow at lower strain rates and steeper at the higher strain rates. Aermet 100 appeared to show a somewhat discontinuous jump in strength at intermediate strain rates, although its actual trend may be less obvious due to the lack of test repetitions.

This figure also includes the strain-rate dependence of ductility, as described by the reduction in cross-sectional area of the necked region observed after fracture. From this Figure, there are some distinct alloy-dependent differences in strain-rate sensitivity on ductility. Specifically, Aermet 100, HP9-4-20M, and 4340M all show slight-to-moderate loss in ductility as strain-rates increase from quasi-static to dynamic. Aermet 100, which shows the most significant loss of ductility, merely falls from 69% to 61% reduction in area over 6 orders of magnitude in strain-rate. The modest loss of ductility in these alloys is somewhat expected, in correspondence to observed increases in strength. Surprisingly, the ES-1c alloy actually showed significant gains in ductility with strain rate: with reduction-in-area rising from 40% to ~51% over the strain-rate range. These trends will be discussed in the following section.

The fracture surfaces were inspected in the SEM to observe strain-rate dependent changes in fractography. In all cases, the cylindrical tensile bars resulted in a cup-and-cone fracture morphology. In general, the cup-and-cone morphology, illustrated in Figure 7, consists of a “fibrous zone” at the center of the tensile bar associated with early coalescence

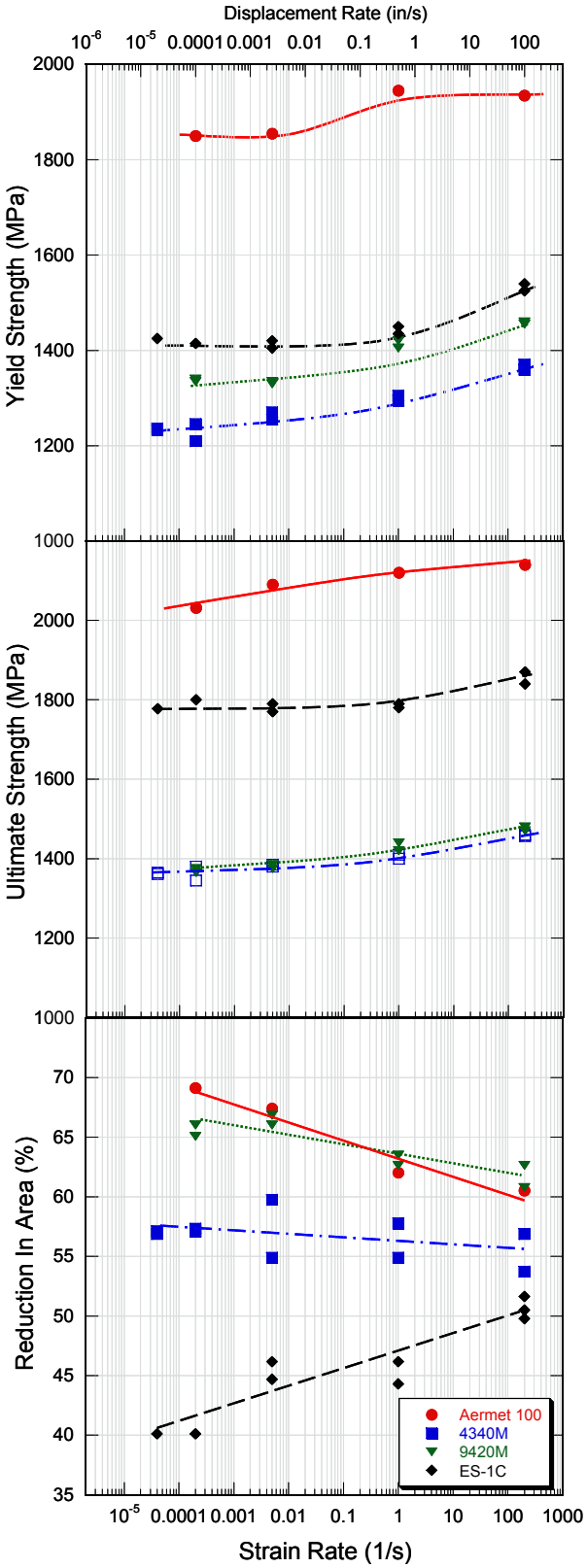

Figure 6. *Tensile property strain-rate trends.*

and slow, stable crack growth, a "radial zone" emanating away from the fibrous zone corresponding to fast, unstable crack propagation, and a "shear-lip zone" around the rim of fracture associated with final failure dictated by the planes of maximum shear ahead of the growing crack tip.

The observed low-magnification fracture surfaces for each of the four alloys are shown in Figure 8 for four strain-rates. Both 4340M and HP9-4-20M exhibit dramatic "radial marks" in the radial zone at slow strain rates, which are not apparent at the faster strain-rates. In the other two alloys, ES-1c and Aermet 100, there are no dramatic radial marks at any strain rate. The only strain-rate dependent fractographic characteristic that was consistent among all four alloys was the relative size of the shear lip, which grows with increasing strain rate.

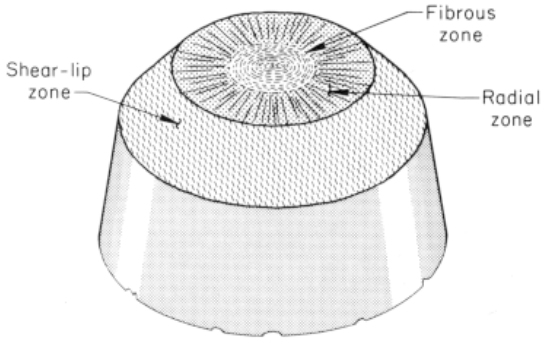

Figure 7. *Schematic of the typical zones associated with failure of cylindrical tensile bars in moderately ductile metals. From [5].*

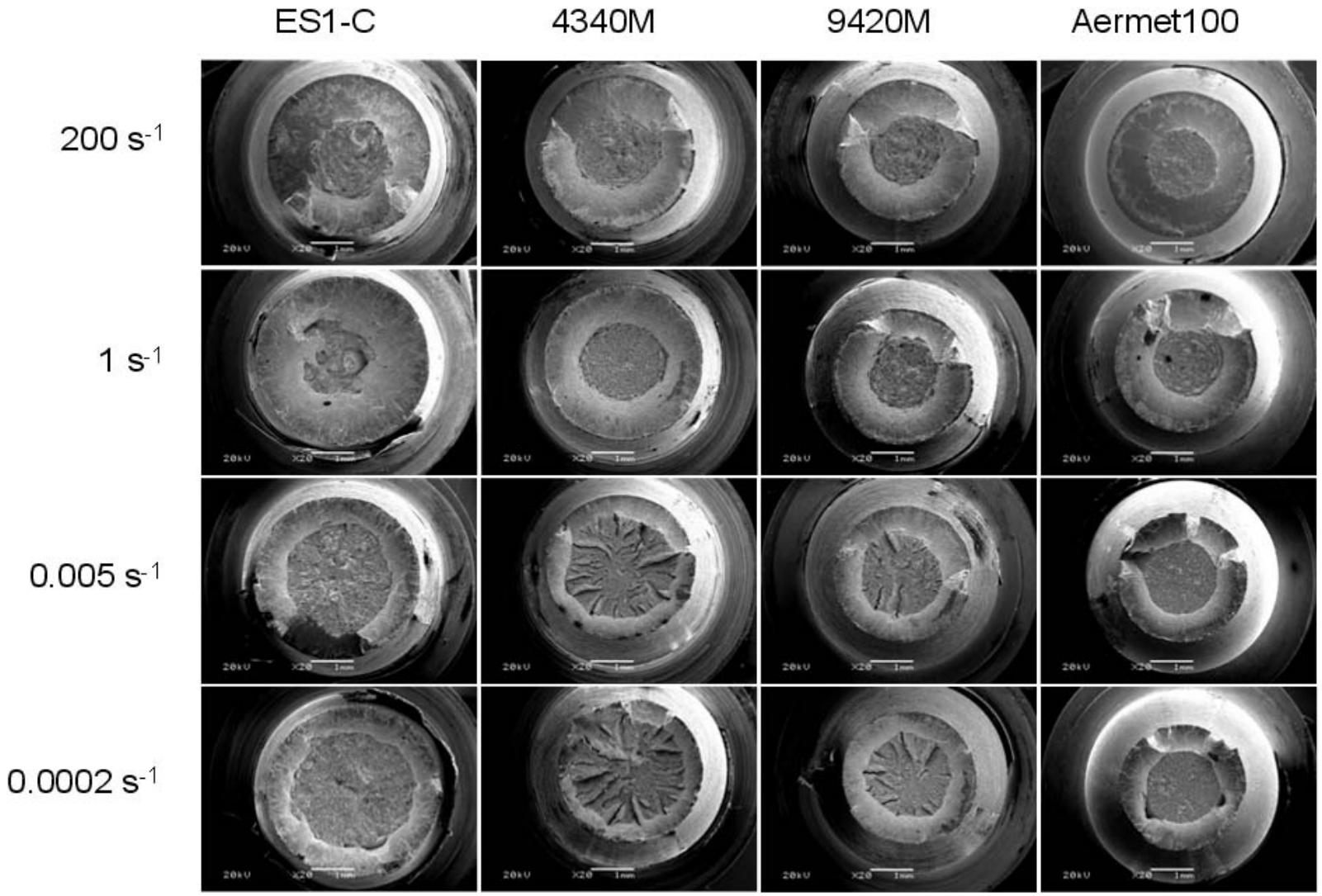

Figure 8. *Low-magnification images of cup-and-cone fracture morphology for the test matrix.*

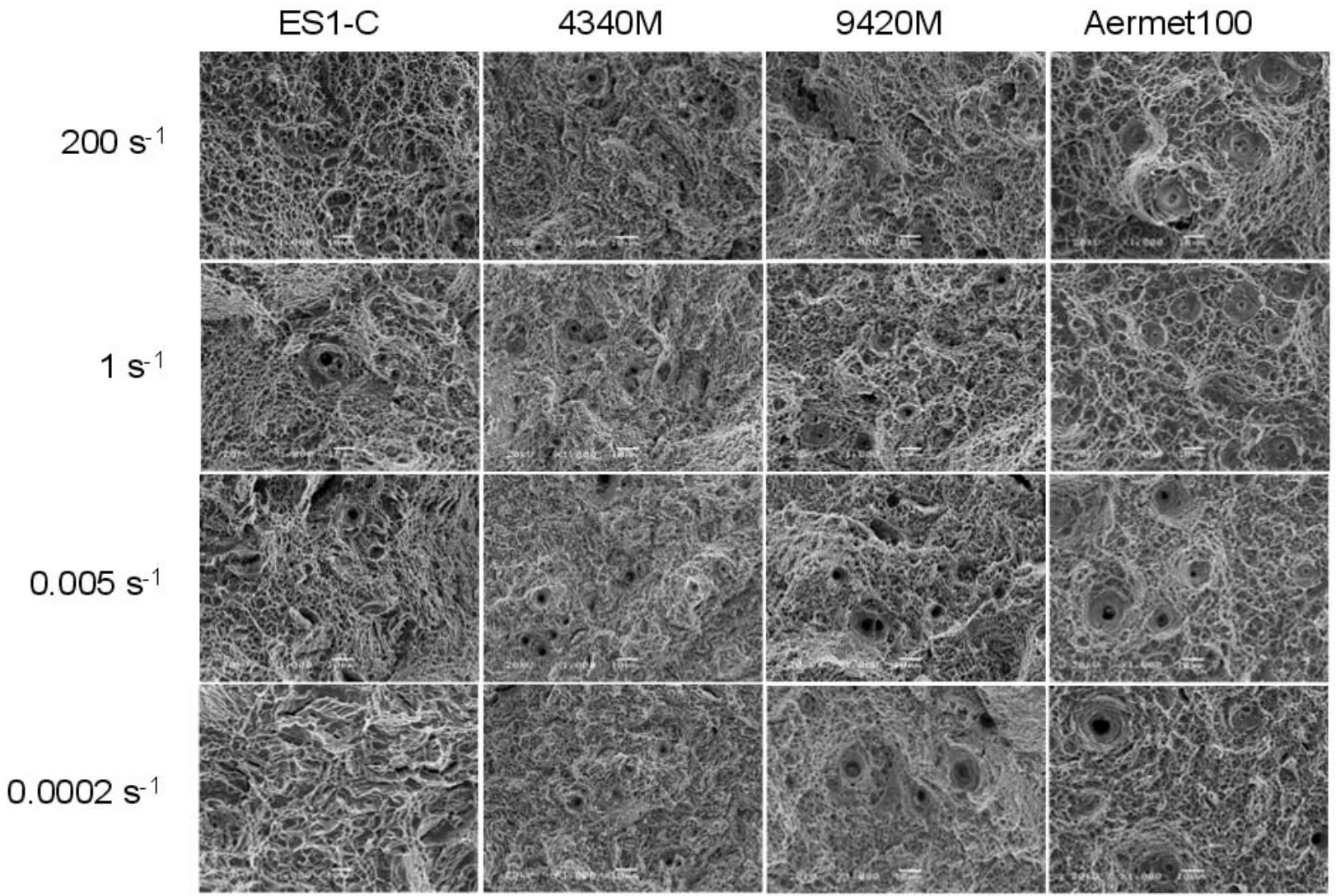

Figure 9. *High-magnification of the ductile dimples in the fibrous zone of the tensile fracture surfaces.*

An accompanying set of higher magnification fractographs were included to assess the morphology of the fibrous zones, as shown in Figure 9. In general, all conditions resulted in a typical microvoid coalescence morphology expected in ductile metal fracture. There were subtle differences in the dimple size from alloy-to-alloy but these dimple sizes did not appear to show a notable strain-rate sensitivity. The only condition that differed significantly in morphology from the others was the slowest strain-rate of the ES-1c alloy (lower-left of Figure 9), where the dimples were less pronounced and more cleavage-like, consistent with the lowest ductility (40% reduction-in-area) observed in that alloy at that strain-rate.

5. Discussion: Constitutive Models for Strain-Rate Sensitivity

The most common generalized description of strain-rate sensitivity is of the following form:

$$\sigma = K\dot{\varepsilon}^{m}$$

where the material's flow stress, σ, is a function of the strain-rate $\dot{\varepsilon}$, material constant K, and strain-rate sensitivity factor m. This relationship presumes a linear relationship between the flow stress and the logarithm of strain-rate. A least squares fit of the yield strength variation with strain-rate is shown for each of the four alloys in Figure 10. Among the four alloys, the strain-rate sensitivity factors m are similar, ranging from 0.004-0.007. These values are quite low compared to most metals which typically fall in the range of 0.02 to 0.2 [4]. It is interesting to note that both the present results, and the prior work of Bleck and Schael shown in Figure 1 exhibit a generally nonlinear trend: the strain-rate sensitivity is shallow at slow strain-rates and appears to rise with increasing strain-rate. Such a relationship is not predicted by the previous equation. This super-exponential strain-rate sensitivity has also been seen in other studies such as the compression testing of interstitial free steel [6].

Perhaps the clearest picture of the super-exponential behavior was found in the work of Campbell and Ferguson in 1970 [7]. They examined strain-rate sensitivity of mild steel at a range of temperatures from 195-713K. Based on their observations they suggested that at strain-rates below ~5000 s^{-1}, there were two regimes of strain-rate sensitivity. At slower-strain rates or higher temperatures, flow is controlled by long-range obstacles to dislocation motion (Region I) and is largely strain-rate insensitive. At lower temperatures or higher

strain-rates, weaker short range obstacles become controlling due to the time-dependent diffusion-limited mechanisms such as climb which are necessary to overcome these short-range obstacles (Region II), leading to a stronger strain-rate dependence.

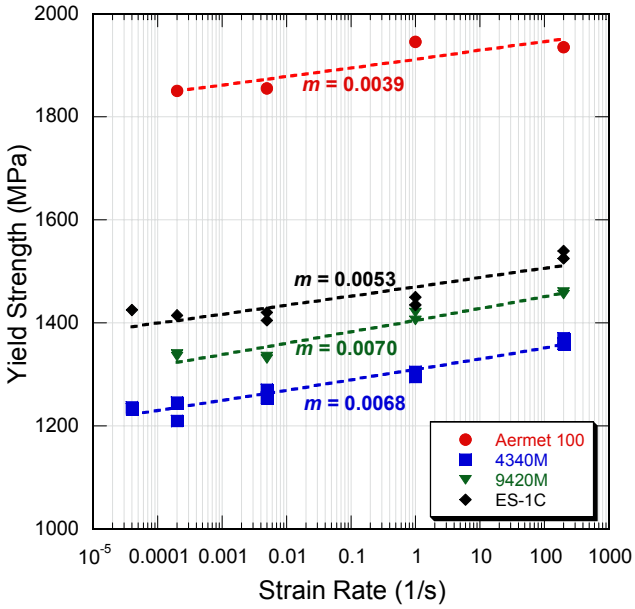

Figure 10. *A traditional exponential relationship between the strain-rate and the yield strength produces an approximate description of observed behavior.*

There are many constitutive flow models which include strain-rate sensitivity, including the Johnson-Cook model, Zerilli-Armstrong Model, Mechanical Threshold Stress Model, and the BCJ Model. Within the limited range of the present study, a thorough evaluation of these models is not productive. However, a much more complete summary of these models is included in a strain-rate sensitivity study on sheet steels [8].

6. Summary: Implications for Designers

Designers typically select alloys based on their quasi-static properties, and assess their designs, such as through the use of finite elements, based on these same quasi-static properties. The present results highlight that the four high-strength steels experience only modest degrees of strain-rate sensitivity. This observation has also recently been made on other high-strength high-toughness steels, including AF1410, PH13-8 Supertough, Hytuf, and conventional HP9-4-20. Specifically, these alloys only exhibit a ~10% increase in yield strength when strain-rates are increased from quasi-static to 200 s^{-1}, and their work-hardening rate is essentially unaffected by strain-rate. This is in distinct contrast to recent results on a very different metallic alloy, eutectic lead-tin solder, where the same range in strain-rates causes a 100% increase in yield-strength. Based on these observations, the use of quasi-static property data for assessing these steels seems reasonable. In the case of the high-strength steels, the small changes in their flow constitutive curve could be incorporated

into future finite element models for slightly increased fidelity. Certainly the very weak strain-rate dependence in these high-strength steels would be no cause for reassessing material selection. Perhaps the most notable consideration in materials selection is the observation that while Aermet100 and HP9-4-20M exhibited a ~10% loss of tensile ductility, the developmental ES-1c alloy exhibited a ~25% gain in tensile ductility at the fastest strain rate of 200 s^{-1} compared to the slowest rate of 0.0002 s^{-1}, a trend which defies explanation based on this study alone. Nevertheless, the Aermet 100 and HP9-4-20M alloys still retain more ductility at 200 s^{-1} than the other two alloys – so materials selection would still favor these alloys in spite of their strain-rate dependent loss in ductility. This does suggest that the materials fracture toughness may itself be diminishing with strain-rate: a possibility which will be examined in a future study.

7. References

1. W. Bleck and I. Schael, "Determination of crash-relevant material parameters by dynamic tensile tests", *Steel Research*, vol.71, no.5, p.173-8, 2000.

2. B.L. Boyce, C.V. Robino, J. Hickerson, and M. Dillmore, "Survey of Case Materials for Earth Penetrating Weapons", Sandia National Laboratories report, SAND2004-1680, 2004.

3. B.L. Boyce and T.B. Crenshaw, "Servohydraulic methods for mechanical testing in the sub-Hopkinson rate regime up to strain rates of 500 1/s", Sandia National Laboratories report, SAND2005-5678, 2005.

4. R.W. Hertzberg, *Deformation and Fracture Mecahncis of Engineering Materials, 3rd Edition*, John Wiley & Sons, New York, 1989.

5. *Metals Handbook, Vol. 9 Fractography and Atlas of Fractographs, 8th Edition,* American Society for Metals, 1974.

6. M. Militsky, "Effects of pre-strain on the mecahncial properties of low-carbon steels tested over a wide range of strain rates," M.S. Thesis, Colorado School of Mines, 2000.

7. J.D. Campbell and W.G. Ferguson, "The temperature and strain-rate dependence of the shear strength of mild steel", Phil. Mag., vol. 21, 1970, pp. 63-82.

8. D. Bruce, "Dynamic tensile testing of sheet steels and influence of strain rate on strengthening mechanisms in sheet steels", Ph.D. Thesis, Colorado School of Mines, 2003.

Distribution

10	MS0889	Brad L. Boyce	1824
1	MS1159	Scott C. Jones	1344
1	MS0889	John J. Stephens	1825
5	MS1160	Vincent K. Luk	5431
1		Michael J. Forrestal	2123
1	MS0325	Danny J. Frew	2615
1	MS0889	Jon Custer	1824
1	MS0889	F. Michael Hosking	1813
3	MS0889	Thomas Crenshaw	1824
2	MS9018	Central Technical Files	8944
2	MS0899	Technical Library	4536
1	MS0161	Patent & Licensing Office	11500
1	MS0123	LDRD Donna Chavez	1011

1 Morris Dilmore (AFRL)
5948 Jack Stokes Road
Baker, FL 32531